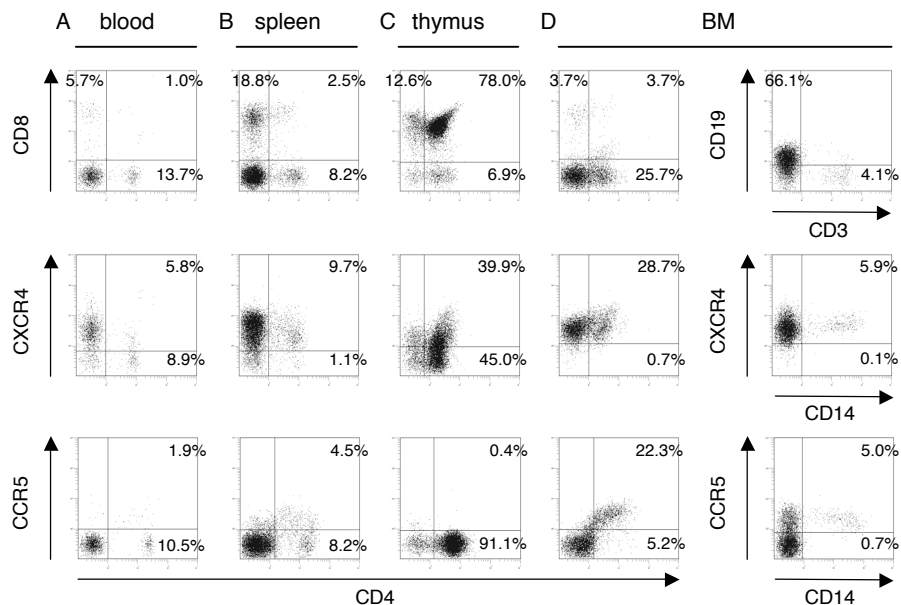


## Infectious disease model

### • HIV-1 infection

1. Watanabe S, Ohta S, Yajima M, et al. Humanized NOD/SCID/IL2Rgamma(null) mice transplanted with hematopoietic stem cells under nonmyeloablative conditions show prolonged life spans and allow detailed analysis of human immunodeficiency virus type 1 pathogenesis. *J Virol.* 2007;81:13259-13264.
2. Watanabe S, Terashima K, Ohta S, et al. Hematopoietic stem cell-engrafted NOD/SCID/IL2Rgamma null mice develop human lymphoid systems and induce long-lasting HIV-1 infection with specific humoral immune responses. *Blood.* 2007;109:212-218.



**Figure 1. Surface expression of HIV-1 coreceptors on CD4<sup>+</sup> cells in various organs of mice 4 months after transplantation.**

A representative FACS profile of human CXCR4 and CCR5 on CD4<sup>+</sup> cells shows the existence of CXCR4<sup>+</sup>CD4<sup>+</sup> and CCR5<sup>+</sup>CD4<sup>+</sup> cells in blood (A), spleen (B), and BM (D), but no CCR5<sup>+</sup>CD4<sup>+</sup> cells in the thymus (C). BM results show that many CD4<sup>+</sup> cells are neither CD3<sup>+</sup> T cells nor CD14<sup>+</sup> monocytes. A gate was set on the human CD45<sup>+</sup> population.

**Table 1. Comparison of viral RNA copies in plasma and HIV-DNA copies in the spleen, BM, and thymus from hNOG mice receiving low- and high-dose viral inoculations**

Mouse ID no.	HIV strain	TCID <sub>50</sub>	Time after inoculation, d	RNA viral copies/mL	CD4/CD8 ratio	HIV-DNA copies/10 <sup>6</sup> human cells		
						Spleen	BM	Thymus
<b>Low-dose viral inoculation group</b>								
113-1	HIV-1 <sub>JRCSF</sub>	200	18	6 240	1.8	34 177	11 785	3 495
112-2	HIV-1 <sub>JRCSF</sub>	200	18	<500	1.2	< 100	< 100	< 100
113-2	HIV-1 <sub>JRCSF</sub>	200	40	6 177	1.6	25 855	27 920	3 473
112-3	HIV-1 <sub>JRCSF</sub>	200	40	<500	0.9	< 100	< 100	<100
112-4	HIV-1 <sub>MNp</sub>	180	18	72 477	1.3	18 873	100	ND
113-4	HIV-1 <sub>MNp</sub>	180	40	70 667	0.3	4 947	653	32 163
112-1	HIV-1 <sub>MNp</sub>	180	40	<500	0.9	< 100	< 100	< 100
<b>High-dose viral inoculation group</b>								
136-3	HIV-1 <sub>JRCSF</sub>	65 000	25	252 381	0.8	958 871	1 797 600	232 155
136-2	HIV-1 <sub>JRCSF</sub>	65 000	29	50 167	0.7	41 172	54 521	8 600
141-1	HIV-1 <sub>JRCSF</sub>	65 000	30	67 667	2.2	27 735	52 430	429
161-3	HIV-1 <sub>JRCSF</sub>	65 000	30	13 847	0.9	104 466	14 653	111 080
157-3	HIV-1 <sub>MNp</sub>	20 000	31	1 253 925	0.5	41 053	56 802	976 556
157-4	HIV-1 <sub>MNp</sub>	20 000	31	147 973	0.6	3 634	262	40 796
161-6	HIV-1 <sub>MNp</sub>	20 000	31	108 073	1.7	4 991	< 100	3 673

Seven mice inoculated with a low infection dose of HIV-1<sub>JRCSF</sub> (200 TCID<sub>50</sub>) or HIV-1<sub>JRCSF</sub> (180 TCID<sub>50</sub>), and 7 mice receiving a high dose of HIV-1<sub>JRCSF</sub> (65,000 TCID<sub>50</sub>) or HIV-1<sub>JRCSF</sub> (20,000 TCID<sub>50</sub>) were listed. ND indicates not done.

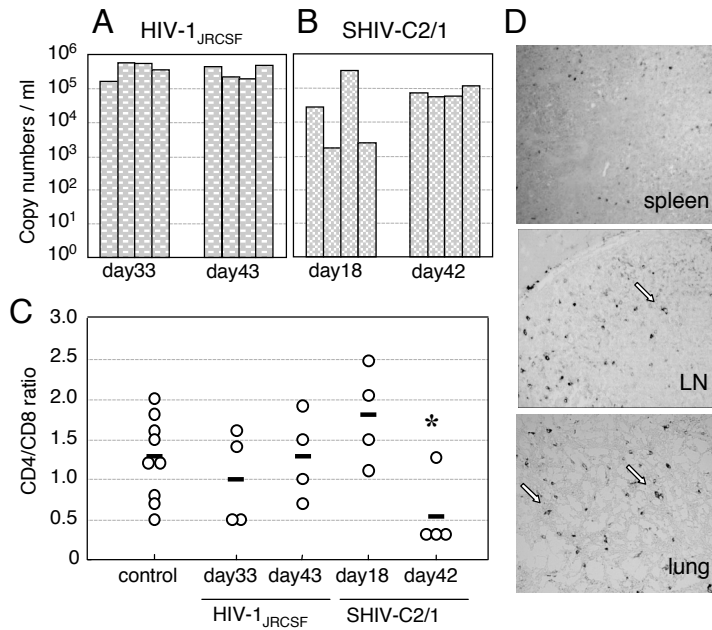


**Figure 2. The numbers of RNA viral copies in plasma, CD4<sup>+</sup>/CD8<sup>+</sup> T-cell ratios in the spleen, and p24 detection in the immunohistochemistry of HIV/SHIV-infected mice.**

(A) Viral copy numbers of 8 mice inoculated with a high infectious dose of HIV-1<sub>JRCSF</sub> (65,000 TCID<sub>50</sub>) and killed on days 33 and 43 after inoculation. (B) Viral copy numbers of 8 mice inoculated with a high infectious dose of SHIV-C2/1 (50,000 TCID<sub>50</sub>) and killed on days 18 and 42 after inoculation. Note that all the mice showed high levels of viremia that lasted more than 40 days after inoculation. (C) CD4/CD8 cell ratios in the spleens of 16 infected mice and 9 uninfected control mice. Control mice were not inoculated with HIV/SHIV and were killed on days 105 to 166 after stem cell transplantation. There was no significant rapid loss of CD4<sup>+</sup> cells in HIV-1<sub>JRCSF</sub>-infected mice, while a decline of the CD4/CD8 ratio was detected in SHIV-C2/1-infected mice on day 42 after infection compared with uninfected control mice (\*P < .05). The short bars indicate the means of each group. (D) P24<sup>+</sup> cells are clearly observed in the spleen, LNs, and lungs. Arrow indicates p24 positive for macrophage-like cells. Original magnification, x100.

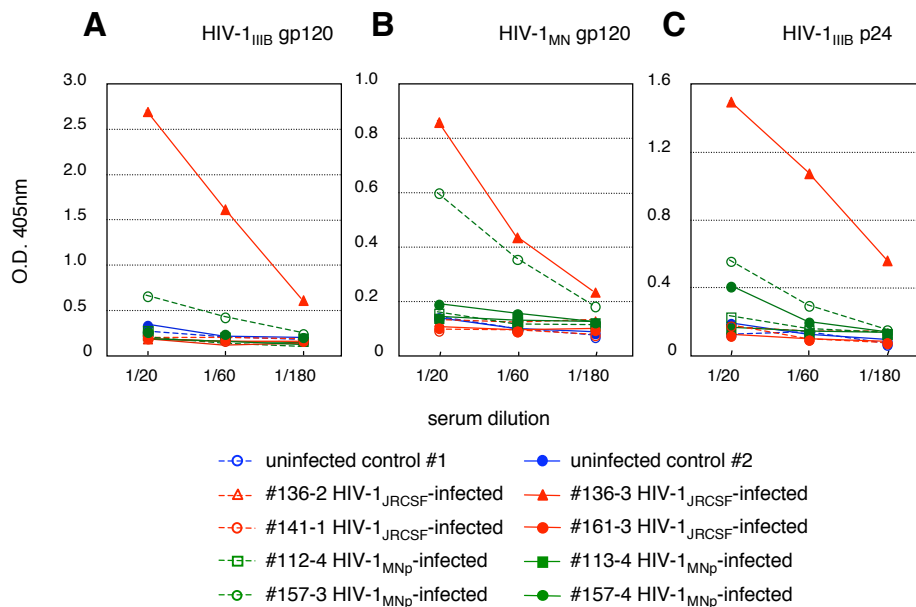


**Figure 3. Detection of anti-HIV-1 antibodies from the plasma of HIV-1-infected mice.**

An ELISA assay was conducted by using plasma from 14 mice inoculated with either HIV-1<sub>JRCSF</sub> or HIV-1<sub>MNP</sub>, and from 2 uninfected control mice. Representatives (n = 8) of the 14 HIV-1-inoculated mice, and the 2 uninfected mice, are shown in the panels. Measurements of specific human antibodies for HIV-1<sub>IIB</sub> gp120 (A), HIV-1<sub>MN</sub> gp120 (B), and HIV-1<sub>IIB</sub> p24 antigens (C) were shown. Results are expressed as the means from triplicate assays in 3 different experiments.

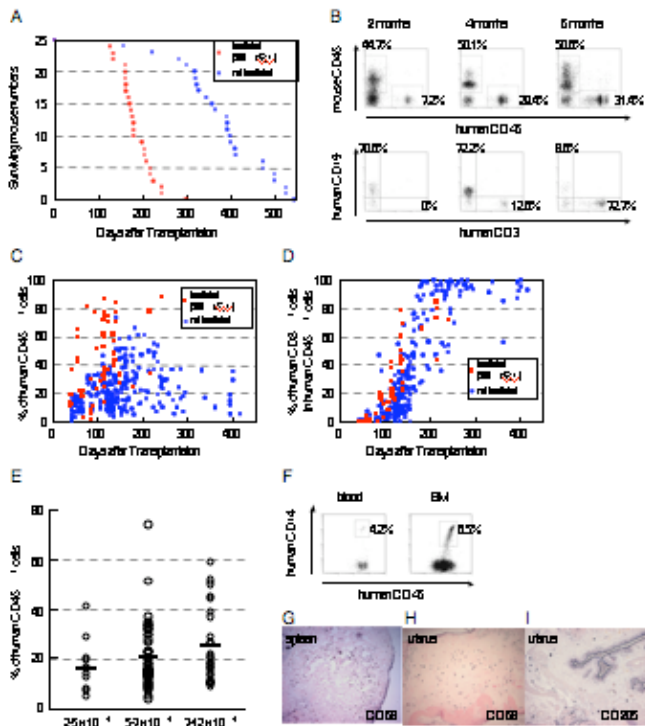
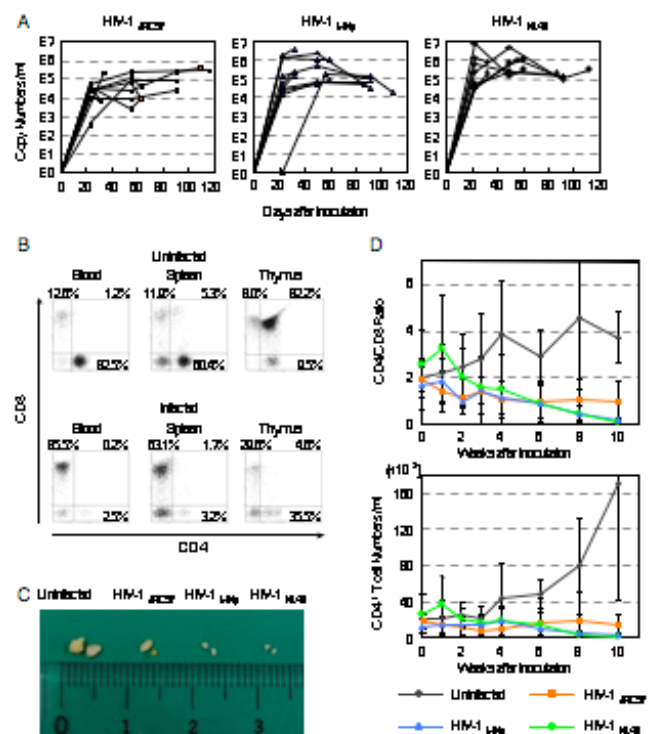


**Figure 4. Human cell generation in hematopoietic stem cell-engrafted hNOG mice with or without myeloablation.**

Life spans of NOG mice transplanted with human stem cells after receiving 300 cGy irradiation ( $n = 25$ ) or not receiving irradiation ( $n = 25$ ). (B) Representative flow cytometric profiles of the mice from 2 to 6 months after transplantation without irradiation. The ratio of human to murine CD45<sup>+</sup> cells and that of human CD3<sup>+</sup> cells to CD19<sup>+</sup> cells are shown. Note that the mice generated human CD45<sup>+</sup> leukocytes that eventually developed human CD19<sup>+</sup> B cells first and then CD3<sup>+</sup> T cells. (C and D) Percentages of human CD45<sup>+</sup> cells (C) and CD3<sup>+</sup> T cells in human CD45<sup>+</sup> cells (D) in peripheral blood from 65 mice that received 300 cGy irradiation and 222 nonirradiated mice 40 to 413 days after transplantation. (E) Summary of engraftment levels in nonirradiated mice transplanted with  $2 \times 10^4$  to  $5 \times 10^4$  cells ( $n = 11$ ),  $5 \times 10^4$  to  $7 \times 10^4$  cells ( $n = 53$ ), or  $7 \times 10^4$  to  $12 \times 10^4$  ( $n = 30$ ) human stem cells. Percentages of human CD45<sup>+</sup> leukocytes in peripheral blood during 4 to 5 months after transplantation were shown. The horizontal black bars indicate the averages of the groups. (F to I) Flow cytometric analysis and immunohistochemical analysis of the expression of myelomonocytic markers in nonirradiated mice 4 months after transplantation. Human CD14<sup>+</sup> monocytes/macrophages were recognized in peripheral blood and BM (F). A gate was set on the human CD45<sup>+</sup> population. Human CD68<sup>+</sup> macrophages and CD205<sup>+</sup> DCs were also detected in spleen (G) and uterus (H and I). Visualization was performed with 5-bromo-4-chloro-3-indolylphosphate (BCIP). The original magnifications were  $\times 100$  (G and H) and  $\times 200$  (I).

**Figure 5. Long-lasting viremia and CD4<sup>+</sup> T-cell depletion in R5- and X4-tropic HIV-1-infected hNOG mice.**

(A) Viral copy numbers in plasma from 29 mice intravenously inoculated with R5-tropic HIV-1<sub>JRC5F</sub> (65,000 TCID<sub>50</sub>;  $n = 11$ ), X4-tropic HIV-1<sub>MNP</sub> (20,000 TCID<sub>50</sub>;  $n = 10$ ), and X4-tropic HIV-1<sub>NL4-3</sub> (60,000 TCID<sub>50</sub>;  $n = 8$ ). RNA viral copy numbers were measured using a real-time PCR quantification assay as previously described (22). (B) The percentages of CD4<sup>+</sup> CD8<sup>+</sup> (top left), CD4<sup>+</sup> CD8<sup>+</sup> (top right), and CD4<sup>+</sup> CD8<sup>-</sup> (bottom right) cells in blood, spleen, and thymus from a uninfected control mouse and a V-1<sub>NL4-3</sub>-infected mouse (32 days postinfection). These two mice were constructed with HSCs from the same cord blood donor, and sacrificed 181 and 169 days after transplantation, respectively. A gate was set on the human CD45<sup>+</sup> population. (C) Comparison of the apparent size of mesenteric LN from uninfected mice or mice infected with HIV-1<sub>JRC5F</sub> (109 days postinfection), HIV-1<sub>MNP</sub> (109 days postinfection), or HIV-1<sub>NL4-3</sub> (112 days postinfection). A uninfected control mouse was sacrificed 249 days after transplantation, and three HIV-1-infected mice were sacrificed 246, 246, and 249 days after transplantation. (D) Comparison of CD4/CD8 T-cell ratios and absolute CD4<sup>+</sup> T-cell numbers in peripheral blood from uninfected control mice ( $n = 7$ ), R5-tropic HIV-1<sub>JRC5F</sub>-infected mice ( $n = 7$ ), X4-tropic HIV-1<sub>MNP</sub>-infected mice ( $n = 5$ ), and X4-tropic HIV-1<sub>NL4-3</sub>-infected mice ( $n = 6$ ). Results are expressed as means  $\pm$  standard deviations (error bars).



## Infectious disease model

### • ATL infection

Dewan MZ, Terashima K, Taruishi M, et al. Rapid tumor formation of human T-cell leukemia virus type 1-infected cell lines in novel NOD-SCID/gammac(null) mice: suppression by an inhibitor against NF-kappaB. *J Virol.* 2003;77:5286-5294.

We established a novel experimental model for human T-cell leukemia virus type 1 (HTLV-1)-induced tumor using NOD-SCID/gammac(null) (NOG) mice. This model is very useful for investigating the mechanism of tumorigenesis and malignant cell growth of adult T-cell leukemia (ATL)/lymphoma, which still remains unclear. Nine HTLV-1-infected cell lines were inoculated subcutaneously in the postauricular region of NOG mice. As early as 2 to 3 weeks after inoculation, seven cell lines produced a visible tumor while two transformed cell lines failed to do so. Five of seven lines produced a progressively growing large tumor with leukemic infiltration of the cells in various organs that eventually killed the animals. Leukemic cell lines formed soft tumors, whereas some transformed cell lines developed into hemorrhagic hard tumors in NOG mice. One of the leukemic cell lines, ED-40515(-), was unable to produce visible tumors in NOD-SCID mice with a common gamma-chain after 2 weeks. In vivo NF-kappaB DNA binding activity of the ED-40515(-) cell line was higher and the NF-kappaB components were changed compared to cells in vitro. Bay 11-7082, a specific and effective NF-kappaB inhibitor, prevented tumor growth at the sites of the primary region and leukemic infiltration in various organs of NOG mice. This in vivo model of ATL could provide a novel system for use in clarifying the mechanism of growth of HTLV-1-infected cells as well as for the development of new drugs against ATL.

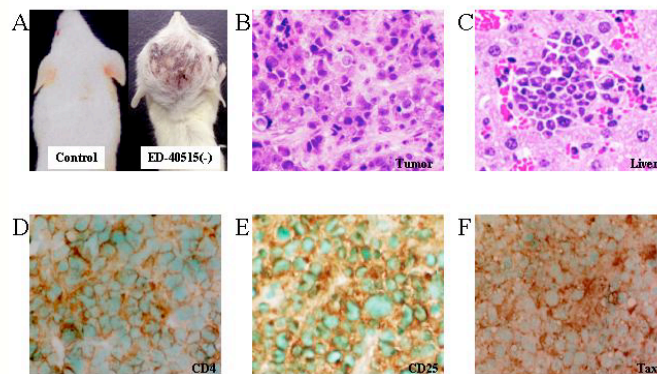


**Figure 6. Tumor growth and infiltration in NOG mice.** (A) Photographs of normal NOG mice and those inoculated with ED-40515(-) cells subcutaneously in the post-auricular region after 3 weeks. Hematoxylin-eosin staining of tumor tissue of an ED-40515(-) injected mouse (B) and a section of the tumor-bearing liver of an SLB-1-inoculated mouse (C). In vivo expression of CD4, CD25 and Tax is revealed by immunohistochemistry. Immunohistochemical staining using anti-CD4 (D) and anti-CD25 (E) was conducted on tumor tissues from mice 2 weeks after inoculation of the ED-40515(-) cell line. Tumor Tissue from mice 2 weeks after inoculation of SLB-1 cell line was stained with anti-Tax antibody (F).

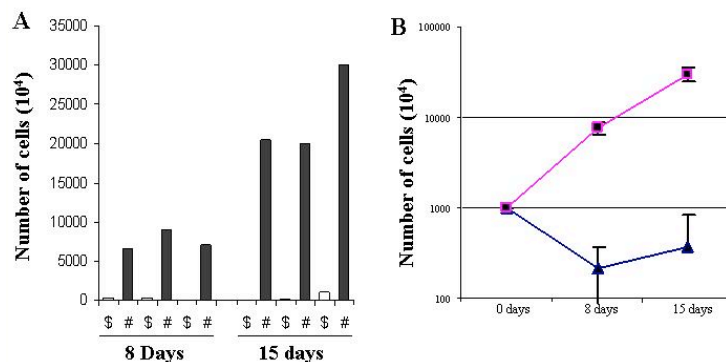


**Figure 7. Comparison of ED-40515(-) cells growth in NOG and NOD-SCID mice.** To evaluate the in vivo growth pattern of tumor cells in SCID mice, we inoculated the ED-40515 (-) cell line in both NOD/SCID and NOG mice. (A) Tumor cells obtained from mice on day 8 and 15 were counted by the trypan blue method. Open and black bars represent the number of cells in individual NOD-SCID (S) and NOG (#) mice, respectively. (B) Mean results +/- s.e. from 3 mice of individual strains on day 8 and 15 (Quadrangle and Rectangle are represented NOD-SCID and NOG mice, respectively).

## Infectious disease model

### • EBV infection model

Yajima M, Imadome K, Nakagawa A, et al. A new humanized mouse model of Epstein-Barr virus infection that reproduces persistent infection, lymphoproliferative disorder, and cell-mediated and humoral immune responses. *J Infect Dis.* 2008;198:673-682.

The functional human immune system, including T, B, and natural killer lymphocytes, is reconstituted in NOD/Shi-scid/IL-2R $\gamma^{\text{null}}$  (NOG) mice that receive hematopoietic stem cell transplants. Here, we show that these humanized mice can recapitulate key aspects of Epstein-Barr virus (EBV) infection in humans. Inoculation with  $\sim 1 \times 10^3$  TD<sub>50</sub> (50% transforming dose) of EBV caused B cell lymphoproliferative disorder, with histopathological findings and latent EBV gene expression remarkably similar to that in immunocompromised patients. Inoculation with a low dose of virus ( $\leq 1 \times 10^1$  TD<sub>50</sub>), in contrast, resulted in apparently asymptomatic persistent infection. Levels of activated CD8<sup>+</sup> T cells increased dramatically in the peripheral blood of infected mice, and enzyme-linked immunospot assay and flow cytometry demonstrated an EBV-specific T cell response. Immunoglobulin M antibody specific to the EBV-encoded protein BFRF3 was detected in serum from infected mice. The NOG mouse is the most comprehensive small-animal model of EBV infection described to date and should facilitate studies of the pathogenesis, prevention, and treatment of EBV infection.

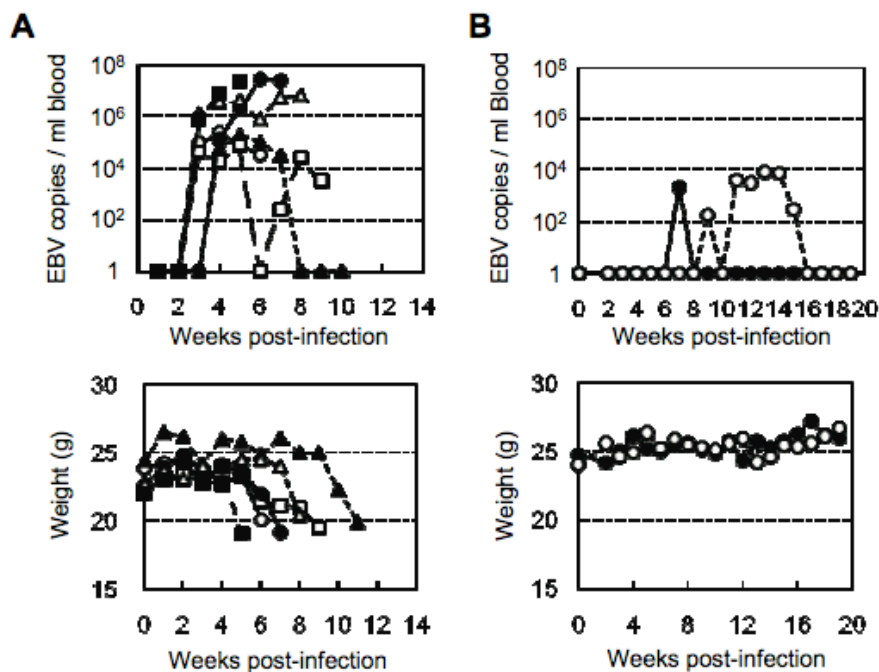


**Figure 1. Peripheral blood Epstein Barr virus (EBV) DNA load and body weight in humanized NOG (hNOG) mice infected with EBV.** A, Infection at a high dose of virus. Six mice were inoculated intravenously with  $1 \times 10^3$  TD<sub>50</sub> of EBV. Peripheral blood EBV DNA load (upper panels) and body weight (lower panels) were then determined weekly. Each symbol in the graphs represents an individual mouse. Interruption of records indicates the death or killing of a mouse. B, Infection at lower doses. Peripheral blood EBV DNA load (upper panel) and body weight (lower panel) of 2 mice inoculated with low doses of EBV (black circle,  $1 \times 10^{-1}$  TD<sub>50</sub>; white circle,  $1 \times 10^1$  TD<sub>50</sub>) are shown.

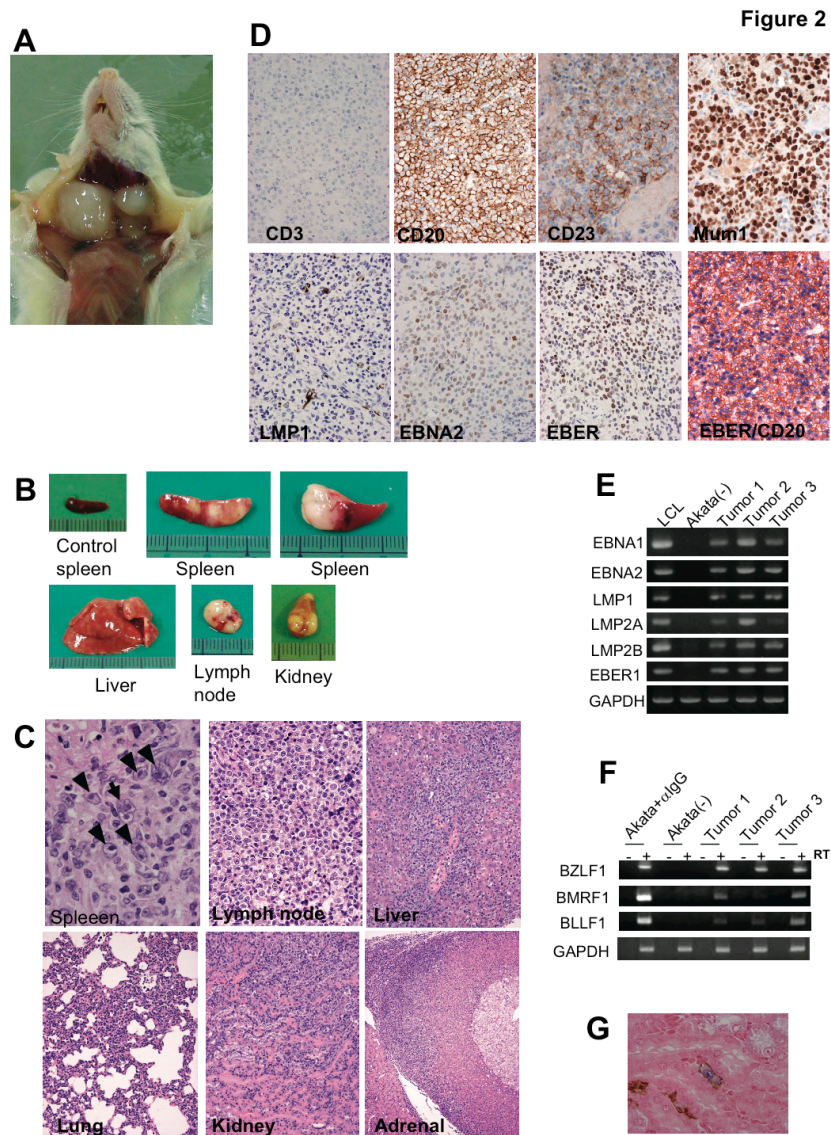


**Figure 2. Pathological and virological analyses of Epstein-Barr virus (EBV)-infected humanized NOG (hNOG) mice.** A, Photograph of an EBV-infected mouse showing tumors in the cervical area. B, Photographs of spleens, liver, lymph node, and kidney from EBV-infected mice with lymphoproliferative disorder. The upper left panel shows the spleen from an uninfected mouse. C, Photomicrographs of hematoxylin-eosin-stained tissues from mice with lymphoproliferative disorder. The arrow indicates a Reed-Sternberg-like cell, and the arrowheads indicate Hodgkin-like cells. Original magnifications,  $\times 1000$  for spleen,  $\times 400$  for lymph node, and  $\times 200$  for liver, lung, kidney, and adrenal gland. D, Immunohistochemical staining for lymphocyte surface markers (CD3, CD20, CD23, and Mum1) and EBV-encoded proteins (latent membrane protein [LMP] 1 and Epstein-Barr nuclear antigen [EBNA] 2), as well as in situ hybridization for EBV-encoded small RNA (EBER), in a lymph node from a mouse with lymphoproliferative disorder. The bottom right panel represents double staining for EBER and CD20. Original magnifications,  $\times 200$  for all except EBER/CD20, which is  $\times 400$ . E and F, Reverse-transcription polymerase chain reaction detection of latent-cycle (E) and lytic-cycle (F) EBV gene expression in tumors from EBV-infected hNOG mice. Spleen tumors from 3 different mice were examined for the expression of EBNA1, EBNA2, LMP1, LMP2A, LMP2B, EBER1, BZLF1, BMRF1, and BLLF1. RNA samples from a lymphoblastoid cell line (LCL) (E) and anti-IgG-treated Akata cells (F) were used as positive controls, and an RNA sample from EBV-negative Akata cells (E and F) was used as a negative control. Assays were done with (+) or without (–) reverse transcriptase (RT) in panel F. Expression of GAPDH was examined as a reference. G, Double staining of EBER and CD20 in the liver of an hNOG mouse that was persistently infected with EBV without developing lymphoproliferative disorder. EBER is stained navy in the nucleus, and CD20 is stained brown in the membrane. Original magnification,  $\times 1000$ .

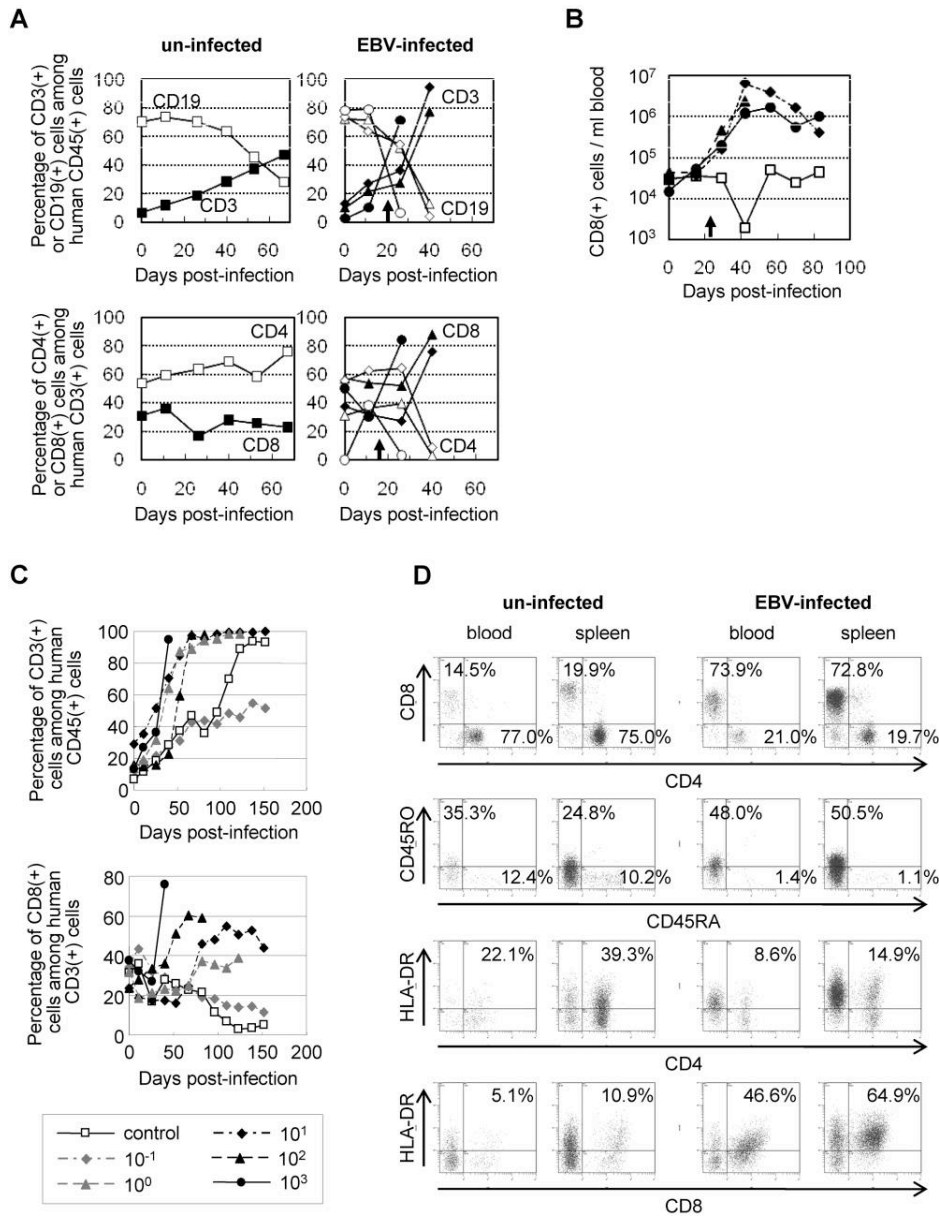


**Figure 3. Surface marker expression by peripheral blood T cells in Epstein-Barr virus (EBV)-infected humanized NOG (hNOG) mice.** A, Changes in the percentages of CD3<sup>+</sup> T cells and CD19<sup>+</sup> B cells among human CD45<sup>+</sup> leukocytes (upper panels) and in the percentages of CD8<sup>+</sup> cells and CD4<sup>+</sup> cells among CD3<sup>+</sup> cells (lower panels) after infection with EBV. Results obtained from 3 EBV-infected mice and an uninfected mice are shown. White symbols indicate the percentage of CD19<sup>+</sup> cells (upper panels) or CD4<sup>+</sup> cells (lower panels); black symbols indicate the percentage of CD3<sup>+</sup> cells (upper panels) or CD8<sup>+</sup> cells (lower panels). A vertical arrow in the graph area shows the time point at which EBV DNA was first detected in peripheral blood. B, Changes in the no. of CD8<sup>+</sup> T cells in the peripheral blood of EBV-infected hNOG mice. White symbols indicate uninfected mice, and black symbols indicate infected mice. Note that cell no. is plotted in a logarithmic scale. C, Viral dose-dependent T cell responses in hNOG mice inoculated with serially diluted EBV. Ten-fold serial dilutions of an EBV sample starting from  $1 \times 10^3$  TD<sub>50</sub> per inoculate were injected intravenously into NOG mice that had undergone transplantation with the same lot of human hematopoietic stem cells (HSCs). Changes in the percentages of CD3<sup>+</sup> T cells among human CD45<sup>+</sup> leukocytes (upper panel) and in the percentages of CD8<sup>+</sup> cells among CD3<sup>+</sup> cells (lower panel) after inoculation with EBV are shown. The viral dose for each mouse is shown in the key. D, Comparison of surface marker expression between EBV-infected mice and control mice. Two mice that underwent transplantation with the same lot of human HSCs were either inoculated with EBV or left uninfected; 10 weeks after inoculation, mononuclear cells obtained from peripheral blood or spleen were gated for the expression of human CD3 and then examined for the expression of CD8 and CD4 (top panels), CD45RO and CD45RA (second from top), HLA-DR and CD4 (second from bottom), and HLA-DR and CD8 (bottom).